Published OnlineFirst April 10, 2014; DOI: 10.1158/2326-6066.CIR-13-0143

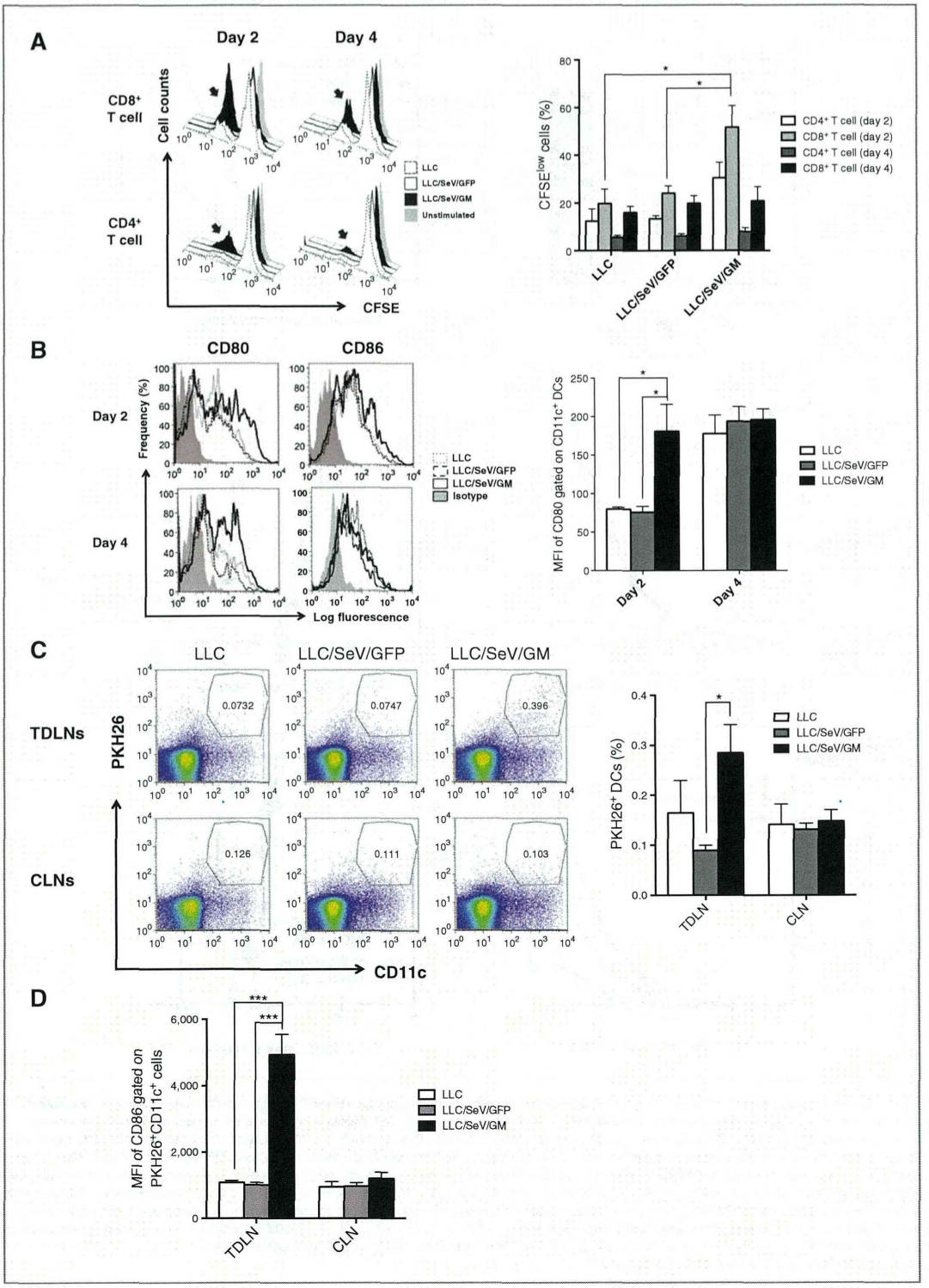

Downloaded from cancerimmunolres.aacrjournals.org on April 19, 2015. © 2014 American Association for Cancer Research.

Published OnlineFirst April 10, 2014; DOI: 10.1158/2326-6066.CIR-13-0143

Table 1. Canonical pathways identified by IPA

Pathways	−log (*P* value)	Molecules
Role of pattern recognition receptors in recognition of bacteria and viruses	7.42E+00	OAS1, C3, OAS2, IL6, CCL5, Oas1f, OAS3, IFNA1/IFNA13, TLR2, IFIH1, IRF7, DDX58, TLR7, PIK3R6, EIF2AK2
Pathogenesis of multiple sclerosis	5.33E+00	CXCL10, CXCL9, CCL4, CCL5, CXCL11
Activation of IRF by cytosolic pattern recognition receptors	4.38E+00	DHX58, IFIH1, IRF7, DDX58, ZBP1, STAT2, IL6, IFIT2, IFNA1/IFNA13, ISG15
IFN signaling	3.96E+00	IFIT3, IFIT1, OAS1, MX1, IFI35, STAT2, IFNA1/IFNA13
DC maturation	3.01E+00	FCGR2A, HLA-DMB, IL6, MAPK13, FCGR2B, TREM2, IFNA1/IFNA13, FCGR1A, TLR2, COL1A2, IL1RN, FSCN1, PIK3R6, STAT2
Hepatic fibrosis/hepatic stellate cell activation	2.58E+00	COL1A2, CXCL3, FN1, CXCL9, IGF1, PDGFA, CCL21, CD14, MMP13, CCL5, IL6, IFNA1/IFNA13
Role of hypercytokinemia/hyperchemokinemia in the pathogenesis of influenza	2.49E+00	CXCL10, CCL4, IL1RN, CCL5, IL6, IFNA1/IFNA13
Communication between innate and adaptive immune cells	2.47E+00	CXCL10, TLR2, CCL4, IL1RN, TLR7, CCL5, IL6, IFNA1/IFNA13, Ccl9
Role of tissue factor in cancer	2.45E+00	F10, PDIA2, PIK3R6, HCK, MMP13, F7, LIMK2, MAPK13, FGR, F2
LXR/RXR activation	2.26E+00	APOE, SCD, C3, MSR1 (includes EG:20288), IL1RN, LPL, CLU, CD14, IL6, GC

TLR7 agonist enhanced the therapeutic antitumor effects of GVAX therapy using irradiated autologous GM-CSF gene-transduced vaccine cells in both LLC and CT26 tumor-bearing mouse models with augmented pDC activation. These results showed that the combination of GVAX and imiquimod is an effective therapeutic strategy for cancer immunotherapy, and indicate that activated pDCs have a critical role in the GM-CSF–induced induction of antitumor immunity.

Materials and Methods

Mice

Five- to 10-week-old female immunocompetent C57/BL6N and BALB/cN mice were purchased from Charles River Laboratories Japan and housed in the animal maintenance facility at Kyushu University (Fukuoka, Japan). Type I IFN receptor knockout ($IFNAR^{-/-}$) mice were purchased from The Jackson Laboratory. All animal experiments were approved by the Committee of the Ethics on Animal Experiments in the Faculty of Medicine, Kyushu University. Mouse experiments were carried out at least twice to confirm results.

Tumor cell lines

LLC and CT26 cells were purchased from the American Type Culture Collection (ATCC) and passaged for 3 to 4 months after resuscitation. The mouse melanoma cell line (B16F10) was a kind gift from Dr. Shinji Okano (Kyushu University) and was validated as free from *Mycoplasma* infection; no other validations were performed. Both LLC and CT26 cells were validated as free from *Mycoplasma* infection. No other validations were performed; besides, the former were found as free from ectromelia virus. LLC and B16F10 cells were maintained in Dulbecco's Modified Eagle Medium (DMEM; Nakalai Tesque) supplemented with 10% heat-inactivated fetal bovine serum (FBS) and 1% antibiotic mixture (Nakalai Tesque). CT26 was maintained in RPMI-1640 (Nakalai Tesque) supplemented with 10% FBS and 1% antibiotic mixture.

Gene transduction with nontransmissible recombinant Sendai virus vectors

LLC, B16F10, or CT26 cells were infected with nontransmissible Sendai virus vectors encoding green fluorescence protein (GFP) or mouse GM-CSF (SeV/GFP or SeV/GM, respectively), which were prepared by DNAVEC Corp. (6), at the indicated multiplicity of infection (MOI) for 90 minutes (termed as LLC/SeV/GFP, LLC/SeV/GM, B16/SeV/GFP, B16/SeV/GM, or CT26/SeV/GM cells, respectively). They were cultured for 48 hours after viral gene transduction and used for following mouse studies.

Figure 2. GM-CSF–sensitized DCs elicited superior capacities to stimulate T-cell proliferation and to mobilize TAA-phagocytosed mature DCs into TDLNs. A, CFSE-labeled allogeneic MLR assay. Irradiated $CD11c^+$DCs from mice treated with indicated tumor challenge were mixed with CFSE-labeled allogeneic T cells. After 3 days of coculture, the proliferation rates of T cells were assessed by flow cytometric analysis. Representative histograms depict CFSE expression of allogeneic $CD4^+CD3^+$ or $CD8^+CD3^+$ T cells (left). Bar graphs, mean + SEM percentage of CFSE-diluted cells/total indicated T cells (right). B, representative histograms depict frequency distributions of MFI of CD80 or CD86 expression in $CD11c^+$ DCs from indicated mouse groups on day 2 or 4 after the tumor challenge (left). Bar graphs, mean + SEM of MFI of CD80 on DCs in TDLNs (right). C, representative dot plots show $PKH26^+CD11c^+$ cells gated by their FSC/SSC profiles in TDLNs or CLNs (left). Bar graphs, mean + SEM of percentage of $CD11c^+PKH26^+$ cells in TDLNs or CLNs (right). D, bar graphs, mean + SEM of MFI of CD86 expression levels in $PKH26^+CD11c^+$ cells (*, $P < 0.05$; ***, $P < 0.001$).

Downloaded from cancerimmunolres.aacrjournals.org on April 19, 2015. © 2014 American Association for Cancer Research.

Published OnlineFirst April 10, 2014; DOI: 10.1158/2326-6066.CIR-13-0143

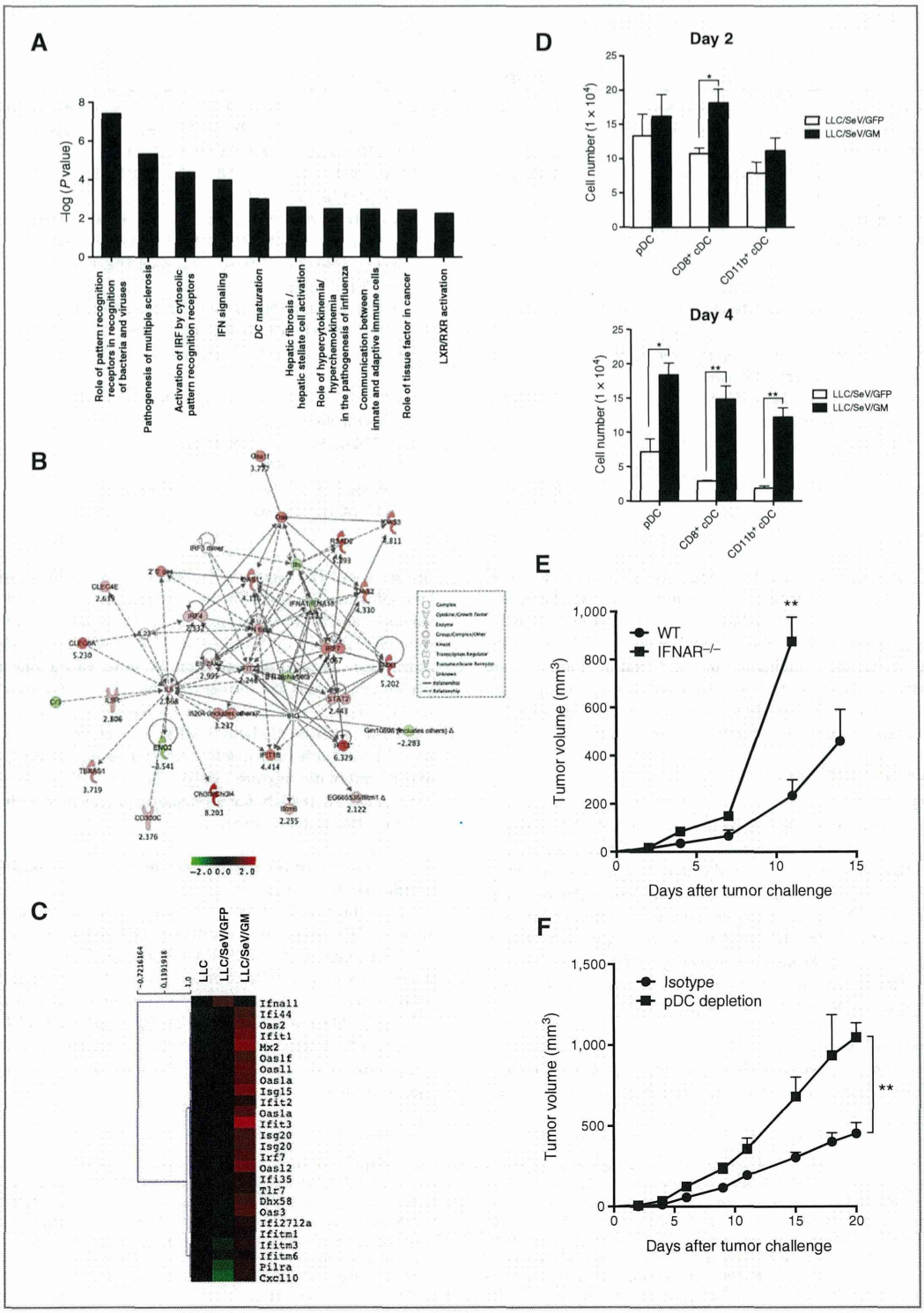

Downloaded from cancerimmunolres.aacrjournals.org on April 19, 2015. © 2014 American Association for Cancer Research.

Published OnlineFirst April 10, 2014; DOI: 10.1158/2326-6066.CIR-13-0143

***In vivo* experiments**

For tumorigenicity assays, syngeneic C57/BL6N mice were subcutaneously challenged with 2.0×10^5 LLC, LLC/SeV/GFP, or LLC/SeV/GM cells with or without imiquimod (R-837; 50 μg/mouse; Invivogen) or lipopolysaccharide (LPS; 5 μg/mouse; Sigma-Aldrich) resuspended in 100-μL Hanks' Balanced Salt Solution (HBSS; Life Technologies) in the right or left flank. To dissect the role of type I IFN and pDCs in the tumorigenicity assays, $IFNAR^{-/-}$ or pDC-depleted mice were subcutaneously challenged with 2.0×10^5 LLC/SeV/GM cells in the right flank. For therapeutic tumor vaccination assays, LLC/SeV/GFP, LLC/SeV/GM, and CT26/SeV/GM cells were irradiated at 50 Gy and were designated as irLLC/SeV/GFP, irLLC/SeV/GM, and irCT26/SeV/GM cells, respectively. On days 2 and 9 after tumor challenge with parental LLC or CT26 cells, C57/BL6N or BALB/cN mice were subcutaneously vaccinated with the indicated tumor vaccine cells in the opposite flank. Tumor volume was measured every 2 to 4 days and calculated with the following formula: $0.4 \times (\text{largest diameter}) \times (\text{smallest diameter})^2$.

ELISA assay

In vitro expression levels of mouse GM-CSF produced from LLC, LLC/SeV/GFP, or LLC/SeV/GM cells at the MOI and time points were measured using mouse GM-CSF enzyme-linked immunosorbent assay (ELISA) kits (R&D Systems).

Flow cytometric analysis

TDLNs, spleen, and tumor vaccine sites (TVS) harvested from the indicated groups of mice ($n = 3$–5) were homogenized and filtered through a 100-μm cell strainer (BD Biosciences). For splenocyte preparation, smashed spleens were treated with ammonium chloride to lyse red blood. For T-cell detection in mixed lymphocyte reaction (MLR) assays, cells were stained with anti-CD4 (RM4.5)–PE (eBioscience), anti-CD3e–APC (145-2C11), and anti-CD8a–PerCP (53-6.7; BioLegend). For phenotypic analyses of DCs in TDLNs, cells were stained with an anti-mouse CD11c Ab [anti-CD11c–APC (N418); BioLegend] in combination with anti-mouse Abs, including anti-B220–PE (RA3-6B2), anti-CD317 (PDCA-1, BST2)–PE (eBio129c; all eBioscience), anti-CD80–PE (16-10A1), anti-CD8a–PerCP, anti-CD86–FITC (GL-1), or anti-CD11b–FITC (M1/70; all BioLegend). For phenotypic analyses of pDCs in TDLNs, cells were stained with either anti-CD317 (PDCA-1, BST2)–PE, anti-PDCA-1–APC (JF05-1C2.4.1; Miltenyi Biotec), or anti-CD11c–PerCPCy5.5 (N418; eBioscience) in combination with anti-mouse Abs, including anti-CD86–FITC, anti-CD9–FITC (MZ3; BioLegend), and anti-Siglec-H–FITC (551.3D3; Miltenyi Biotec). For regulatory T-cell (Treg) detection in TDLNs, cells were permeabilized with Cytofix/Cytoperm kit (BD Biosciences), washed with BD Perm/Wash buffer (BD Biosciences), and stained with anti-CD4, anti-CD25–FITC (PC61.5), and anti-FoxP3–APC (FJK-16s; all eBioscience). Cells were incubated with Abs and analyzed with BD FACSCalibur flow cytometer, CellQuest software (BD Biosciences), and FlowJo software (TreeStar).

Allogeneic MLR assays

To prepare $CD11c^+$ DCs as stimulators, on day 2 of the tumorigenicity assay, $CD11c^+$ DCs were purified from TDLNs in mice treated with LLC, LLC/SeV/GFP, or LLC/SeV/GM cells using CD11c MicroBeads (Miltenyi Biotec). To prepare the pDC subset as stimulators, total bone marrow cells harvested from naïve C57/BL6N mice were cultured in RPMI-1640 supplemented with 50 ng/mL murine Fms-related tyrosine kinase 3 ligand (Flt3L; PeproTech) for 8 days and Siglec-H–positive cells (pDCs) were purified using anti-Siglec-H–FITC Ab and anti-FITC MicroBeads (Miltenyi Biotec). Sorted pDCs were then incubated overnight with or without 2.5 μg/mL of imiquimod or 10 ng/mL of murine recombinant GM-CSF (PeproTech). To prepare allogeneic T cells as responders, T cells were sorted from splenocytes harvested from naïve BALB/cN mice using a Pan T-cell isolation kit II (Miltenyi Biotec). A total of 5.0×10^4 responder T cells labeled with 1.0 μmol/L CFSE [5(6)-carboxyfluorescein diacetate N-succinimidylester; Sigma-Aldrich] were cocultured with an equal number of 30 Gy–irradiated $CD11c^+$ DCs. A total of 2.0×10^5 T cells labeled with 2.5 μmol/L of CFSE were cocultured with 4.0×10^4 of pDCs for 5 days. The proliferation rate of the gated $CD3^+$ T-cell fraction was visualized by CFSE dilution.

Detection of DCs that engulfed TAAs

LLC, LLC/SeV/GFP, and LLC/SeV/GM cells were labeled with the PKH26 Red Fluorescent Cell Linker Mini Kit (Sigma-Aldrich), respectively, according to the manufacturer's instruction. On day 2 after they were subcutaneously injected into the right flanks of mice, axillary lymph nodes in both TDLNs and CLNs were harvested, incubated with anti-CD86–FITC and anti-CD11c–APC Abs, and subjected to flow cytometric analysis.

cDNA microarray

Dead cells were excluded from $CD86^+CD11c^+$ DCs using 7-AAD viability dye (Beckman Coulter), which were sorted by

Figure 3. Transcriptome analysis suggested the involvement of type I IFN–related pathways in GM-DCs during GM-CSF–induced antitumor immunity. A, total RNA was isolated from $CD86^+$ DCs in TDLNs from mice inoculated with LLC, LLC/SeV/GFP, or LLC/SeV/GM cells 2 days after the tumor challenge and subjected to cDNA microarray. The top 10 canonical pathways significantly upregulated in GM-DCs, in comparison with those in GFP-DCs, by which a right-tailed Fisher exact test was calculated using the entire dataset. B, IPA was performed using the type I IFN pathway–related genes from the original commonly regulated probes differentially expressed between GFP-DCs and GM-DCs. Differentially expressed genes are indicated in red and green, representing up- and downregulation induced by GM-CSF activation, respectively. A high degree of gene regulation is indicated by bold-colored genes. Direct or indirect associations with the differentially expressed genes indicated by no color were not found to be significantly different in this assessment. Positive regulatory interactions are depicted by solid arrows (direct interactions) or dashed arrows (indirect interactions). C, heatmap based on type I IFN pathway–related genes that were differentially expressed in $CD86^+$ DCs in TDLNs from indicated mouse groups. D, cell numbers of DC subsets (pDC, $CD8^+$ cDCs, and $CD11b^+$ cDC) in TDLNs at days 2 (top) and 4 (bottom) after the respective tumor challenge were comparatively quantified (*, $P < 0.05$; **, $P < 0.01$). E and F, representative tumor growth curves observed in $IFNAR^{-/-}$ (E) or pDC-depleted (F) mice (**, $P < 0.01$).

Downloaded from cancerimmunolres.aacrjournals.org on April 19, 2015. © 2014 American Association for Cancer Research.

Published OnlineFirst April 10, 2014; DOI: 10.1158/2326-6066.CIR-13-0143

FACSAria (BD Biosciences) from TDLNs of mice on day 2 during the tumorigenicity assay. Cells were transferred to RNA later (Life Technologies) to stabilize and protect intact cellular RNA. RNA isolation was performed according to the TRIzol Reagent technical manual (Life Technologies). Total RNA (50 ng) was amplified and labeled using the Agilent Low-Input QuickAmp Labeling Kit, one color (Agilent Technologies). Labeled cRNA was hybridized to Agilent Whole Mouse Genome Oligo DNA microarray (4 × 44 K) v2 (Agilent Technologies). All gene transcription products were hybridized to microarray slides and were scanned by an Agilent scanner. Relative hybridization intensities and background hybridization values were calculated using the Agilent Feature Extraction Software (v9.5.1.1; Agilent Technologies). The raw signal intensities of two samples were $\log_2$-transformed and normalized by a quantile algorithm with the "preprocessCore" library package on Bioconductor software. We used *Z*-scores to compare significant changes in gene expression in each of the three groups (DCs from mice treated with LLC, LLC/SeV/GFP, and LLC/SeV/GM cells). Lists of genes with statistically significant expression in GM-DCs in comparison with GFP-DCs were submitted to Ingenuity Pathway Analysis (IPA; Ingenuity Systems) and analyzed for overrepresented general functions and the resulting networks. Microarray data were deposited in Gene Expression Omnibus (GEO; http://www.ncbi.nlm.nih.gov/geo/; accession number GSE43169).

In vivo depletion experiments

To deplete pDCs, mice were injected intraperitoneally with 100 μg of anti-PDCA-1 mAb (JF05-1C2.4.1; Miltenyi Biotec) or control Ab (rat IgG; Jackson Immunoresearch), as previously described (7). Effective depletion of PDCA-1$^+$ cells was confirmed by flow cytometric analysis (Supplementary Fig. S1). CD4$^+$ T or CD8$^+$ T cells were depleted by using GK1.5 or 2.43 mAbs, as previously described (8). Briefly, mice received intraperitoneal injections of anti-mouse GK1.5 mAb, anti-mouse 2.43 mAb (50 μg/mouse), or control Ab 6, 4, and 2 days before tumor challenge, and once every 3 days thereafter. Effective depletion of CD4$^+$ and CD8$^+$ T cells was confirmed by flow cytometric analysis (data not shown).

Results

Production of GM-CSF from LLC and B16F10 cells remarkably impaired the tumorigenicity

To test the possibility that substantial secretion of GM-CSF from syngeneic mouse cancer cells facilitates the development of antitumor immune responses, we used recombinant nontransmissible Sendai virus vectors expressing GM-CSF (SeV/GM) at various MOI. Abundant GM-CSF production from the infected LLC (LLC/SeV/GM) cells was observed and was MOI dependent (Fig. 1A). The proliferation rate of LLC cells was not affected by transduction with SeV/GM, as previously described (6). We next performed tumorigenicity assays in which each LLC and LLC/SeV/GM cells (MOI = 1, 10, and 100) were subcutaneously injected into the left flank of syngeneic mice. All mice treated with LLC/SeV/GM cells exhibited significant suppression of the tumor outgrowth in an MOI-dependent manner (Fig. 1B). We thus determined MOI = 100 for gene transduction as an optimized infection dose. Notably, mice treated with LLC/SeV/GM cells showed significantly suppressed tumor growth and prolonged survival of mice, compared with control groups ($P < 0.001$; Fig. 1C). Similar suppression of tumor growth and prolongation of mouse survival were observed when SeV/GM-infected B16F10 melanoma cells were injected to C57BL/6N mice (Fig. 1D).

Increased ability of GM-CSF–sensitized DCs to stimulate T-cell proliferation, accelerate their maturation, and deliver phagocytosed TAAs in TDLNs

To determine a putative phase when GM-CSF–sensitized DCs from TDLNs of mice treated with LLC/SeV/GM cells (GM-DCs) effectively prime naïve T cells, we performed allogeneic MLR assays. GM-DCs exhibited a significantly marked response on day 2 compared with DCs from mice treated with LLC/SeV/GFP cells (GFP-DCs), and stimulated the proliferation of allogeneic CD3$^+$CD4$^+$ T and CD3$^+$CD8$^+$ T cells (Fig. 2A). Furthermore, GM-DCs harvested on day 2 elicited higher expression levels of costimulatory maturation markers *CD80* and *CD86* than those from control mice (Fig. 2B), suggesting that day 2 could be the putative phase to mount optimum immunologic responses by GM-DCs. To explore the migratory capacity of GM-DCs that phagocytosed TAAs at the tumor injection site, we inoculated PKH26-labeled LLC, LLC/SeV/GFP, or LLC/SeV/GM cells into the right flank of mice, and evaluated PKH26$^+$ DC numbers in both TDLNs and contralateral LNs (CLN). The frequencies of PKH26$^+$ DCs in TDLNs, but not CLNs, harvested from mice treated with LLC/SeV/GM cells were significantly increased, indicating that GM-CSF production potentiated the migration of PKH26-labeled LLC cells (TAA)–phagocytosed DCs from the tumor injection site into TDLNs ($P < 0.05$; Fig. 2C). PKH26$^+$ GM-DCs derived from TDLNs, but not from CLNs, showed significantly higher CD86 expression than controls ($P < 0.001$; Fig. 2D).

cDNA microarray analysis revealed the involvement of type I IFN–related pathways in GM-CSF–induced antitumor immunity

On the basis of the aforementioned results, we determined day 2 to be an adequate time point for the peak in T-cell priming by TAA-phagocytosed CD86$^+$ DCs. To address the important factor of DC/T-cell priming, we isolated CD86$^+$ DCs from mice treated with LLC/SeV/GM cells and control groups, and compared the comprehensive gene expression patterns of isolated CD86$^+$ DCs in TDLNs. After normalization of microarray data and statistical analysis, 1,318 genes were found to be differentially expressed between GM-DCs and GFP-DCs with statistical significance (upregulated genes; *Z*-score ≥ 2 and ratio >1.5, downregulated genes; *Z*-score ≤ -2 and ratio <0.66; data not shown). A list of the genes significantly upregulated in the top 10 canonical pathways in CD86$^+$ GM-DCs in comparison with CD86$^+$ GFP-DCs is shown in Table 1. As expected, these genes composed immunologic response–related pathways (Fig. 3A). Among the activated pathways triggered by GM-CSF, we focused on the following representative molecules: IRF7, OAS3 (2′-5′-oligoadenylate synthetase 3), and TLR7, which constitute the type I IFN (IFN-α/IFN-β)–associated pathways (Fig. 3B and C;

Downloaded from cancerimmunolres.aacrjournals.org on April 19, 2015. © 2014 American Association for Cancer Research.

Published OnlineFirst April 10, 2014; DOI: 10.1158/2326-6066.CIR-13-0143

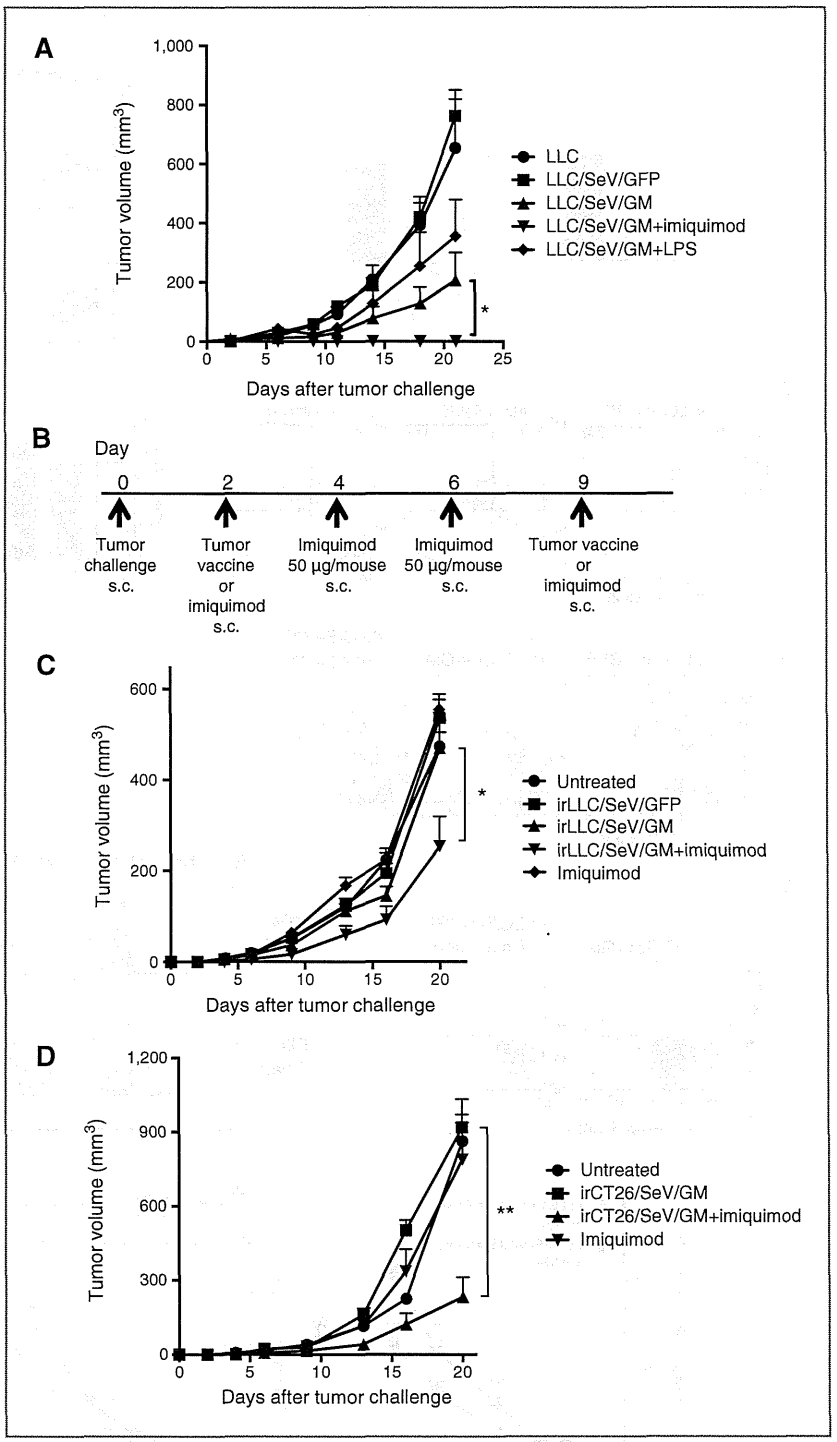

Figure 4. Combined imiquimod and irLLC/SeV/GM cells exert significant therapeutic antitumor effects compared with irLLC/SeV/GM cells alone. A, a total of 2.0×10^5 LLC and LLC/SeV/GM cells with or without LPS or imiquimod were subcutaneously inoculated into the right flanks of C57/BL6N mice. Bar graphs, mean + SEM of tumor volumes. Combined data from two independent experiments with similar results are shown (*, $P < 0.05$). B, schematic diagram of the experimental protocol of therapeutic GM-CSF–based tumor vaccination. Briefly, 2.0×10^5 LLC cells or 3.0×10^5 CT26 cells were inoculated subcutaneously to C57/BL6N or BALB/cN mice. LLC-bearing mice were divided into the following groups: untreated, imiquimod alone, irLLC/SeV/GFP, irLLC/SeV/GM, or irLLC/SeV/GM cells plus imiquimod. CT26-bearing mice were divided into the following groups: untreated, imiquimod alone, irCT26/SeV/GM or irCT26/SeV/GM cells plus imiquimod. On days 2 and 9, mice were inoculated subcutaneously with the indicated vaccine cells. For imiquimod administration, mice were subcutaneously inoculated with imiquimod on days 2, 4, 6, and 9. Represented are tumor growth curves observed in either LLC- (C) or CT26-bearing (D) mice (*, $P < 0.05$; **, $P < 0.01$).

Downloaded from cancerimmunolres.aacrjournals.org on April 19, 2015. © 2014 American Association for Cancer Research.

Published OnlineFirst April 10, 2014; DOI: 10.1158/2326-6066.CIR-13-0143

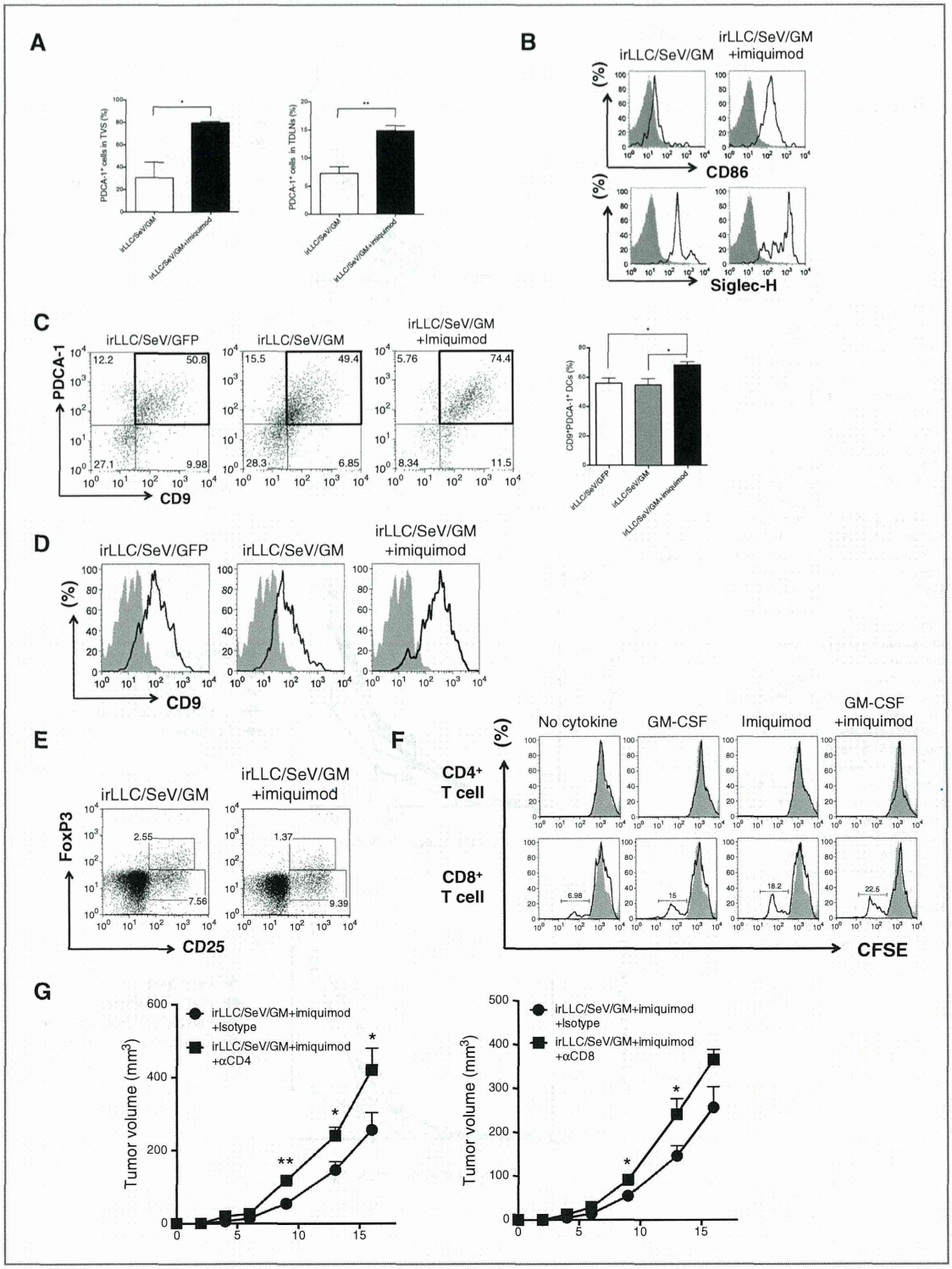

Downloaded from cancerimmunolres.aacrjournals.org on April 19, 2015. © 2014 American Association for Cancer Research.

Published OnlineFirst April 10, 2014; DOI: 10.1158/2326-6066.CIR-13-0143

refs. 5, 9). Microarray results for the expression levels of *Irf7* and *Oas3* were validated by performing qRT-PCR (Supplementary Fig. S2). As pDCs provoke initial defensive antiviral responses by type I IFN production and are the main producers of type I IFNs (10), we speculated that pDCs could be positively involved in the induction of effective GM-CSF–sensitized DC/T-cell priming (11). Indeed, the numbers of pDCs, $CD11b^+$ cDCs, and $CD8^+$ cDCs subsets from total GM-DCs from TDLNs harvested on days 2 and 4 were greater than the equivalent subsets from total GFP-DCs (Fig. 3D). Furthermore, the results of *in vivo* experiments using IFNα receptor knockout ($IFNAR^{-/-}$) mice demonstrated that $IFNAR^{-/-}$ mice inoculated with LLC/SeV/GM cells significantly abrogated the impairment of tumorigenicity seen in the corresponding wild-type (WT) mice (Fig. 3E). Importantly, similar results were also obtained when pDC-depleted mice were used (Fig. 3F). These results collectively demonstrate the positive role of type I IFN–producing pDCs in the induction of GM-CSF–mediated antitumor immunity.

Combination of TLR7 ligand and GM-CSF–secreting LLC cells enhanced the induction of antitumor immunity in both tumorigenicity and therapeutic vaccination models

TLR7-dependent type I IFN pathways are activated by binding with their corresponding ligand, imiquimod (12). To examine the impact of the TLR7-mediated activation of type I IFN–related pathways primarily in pDCs on GM-CSF–induced antitumor immunity, we performed a gain-of-function assay by evaluating the tumorigenicity of LLC/SeV/GM cells with or without imiquimod or TLR4 ligand, LPS, as an irrelevant control. Mice treated with LLC/SeV/GM cells combined with imiquimod showed significantly suppressed tumor development accompanied with complete tumor regression ($P < 0.05$). Conversely, treatment with LLC/SeV/GM cells combined with LPS attenuated the GM-CSF–induced antitumor effects (Fig. 4A), and these mice exhibited no significant changes in body weight (Supplementary Fig. S3). We next attempted to translate these findings into a tumor vaccination therapy by adding imiquimod to the subcutaneous administration of irradiated LLC/SeV/GM (irLLC/SeV/GM) cells to investigate the synergistic effect. Notably, mice treated with combined imiquimod and irLLC/SeV/GM cells elicited a significantly marked suppression of tumor growth of preestablished LLC cells, whereas control mice treated with irLLC/SeV/GM cells or imiquimod alone manifested negligible antitumor effects ($P < 0.05$; Fig. 4B and C). Similarly, mice vaccinated with irradiated GM-CSF gene-transduced (MOI = 100) CT26 colon cancer cells in combination with imiquimod showed significantly suppressed tumor development ($P < 0.01$; Fig. 4D).

Admixed use of TLR7 ligand in combination with GVAX therapy induced pDC activation leading to generation of T-cell–mediated antitumor immunity

To elucidate the effect of imiquimod on GM-CSF–induced initial immune responses, we performed phenotypic immunoanalyses. Six hours after the first tumor vaccination, mice treated with irLLC/SeV/GM cells plus imiquimod showed a significantly higher frequency and number of cells expressing PDCA-1, a pDC-specific marker, than control mice in both TVSs and TDLNs (Fig. 5A and Supplementary Fig. S4). Furthermore, pDCs ($CD11c^+PDCA\text{-}1^+$ cells) derived from mice treated with irLLC/SeV/GM cells plus imiquimod expressed increased levels of CD86 and sialic acid binding Ig-like lectin (Siglec)-H, a functional pDC-specific receptor (Fig. 5B; ref. 13), accompanied with significantly higher levels of serum IFNα (Supplementary Fig. S5). Because $CD9^+$ pDCs stimulated with TLR agonists induced higher amounts of IFNα and provoked protective T-cell–mediated antitumor immunity (14), we compared CD9 expression levels on pDC subsets. Mice treated with irLLC/SeV/GM cells plus imiquimod had significantly increased frequency and mean fluorescence intensity (MFI) of $CD9^+PDCA1^+CD11c^+$ pDCs in TDLNs (Fig. 5C and D). However, the frequency of $CD4^+CD25^+FoxP3^+$ Tregs was decreased in TDLNs from mice treated with irLLC/SeV/GM cells and imiquimod, whereas the frequency of $CD4^+CD25^+FoxP3^-$ T cells was increased in mice treated with combined therapy (Fig. 5E). To investigate the effect of imiquimod and GM-CSF on the T-cell proliferation capacity of pDCs, we performed an allogeneic MLR assay. pDCs stimulated with GM-CSF and imiquimod elicited the most pronounced proliferative activity of $CD8^+$ T cells, but not $CD4^+$ T cells, when compared with controls (Fig. 5F). Moreover, the synergistic therapeutic efficacy of irLLC/SeV/GM cells and imiquimod was significantly inhibited when the corresponding mice were depleted of $CD4^+$ or $CD8^+$ T cells (Fig. 5G).

Discussion

This study demonstrates that SeV/dF-mediated exogenous expression of GM-CSF caused poor growth of cancer cells in

Figure 5. Mice vaccinated with combined irLLC/SeV/GM cells and imiquimod augmented the recruitment of activated pDCs in TDLNs. A, 6 hours after the first tumor vaccination, infiltrating lymphocytes in TVSs or TDLNs were harvested from indicated mouse groups. Bar graphs, mean + SEM of frequency of $PDCA\text{-}1^+$ cells gated on FSC/SSC profiles. B, histograms represent expression levels of Siglec-H or CD86 expression on $CD11c^+PDCA\text{-}1^+$ cells (pDCs) in TDLNs from indicated mouse groups (tinted light gray, isotype control; bold line, anti-CD86 or anti-Siglec-H Ab. C, on day 12, TDLNs were harvested from mice treated with irLLC/SeV/GFP, irLLC/SeV/GM, or irLLC/SeV/GM cells plus imiquimod ($n = 3$). Representative dot plots depict CD9 and PDCA-1 expression gated on $CD11c^+$ cells in TDLNs (left). Bar graphs, mean + SEM of frequency of $CD9^+PDCA\text{-}1^+$ cells on DCs (*, $P < 0.05$; right). D, histograms depict MFI representing CD9 expression levels on $PDCA\text{-}1^+CD11c^+$ subpopulations in TDLNs (tinted light gray, isotype control; bold line, anti-CD9 Ab). E, representative dot plots illustrate CD25 and FoxP3 expression gated on $CD4^+$ T cells in TDLNs from indicated mouse groups. F, CFSE-labeled allogeneic MLR assay. Bone marrow–derived pDCs treated with GM-CSF or imiquimod or in combination with GM-CSF plus imiquimod were mixed with CFSE-labeled T cells. Representative histograms show CFSE expression of allogeneic $CD4^+CD3^+$ or $CD8^+CD3^+$ T cells stimulated by the indicated pDCs. G, tumor growth curves in $CD4^+$ T-cell (left)– or $CD8^+$ T-cell (right)–depleted mice treated with irLLC/SeV/GM cells plus imiquimod (*, $P < 0.05$; **, $P < 0.01$).

Downloaded from cancerimmunolres.aacrjournals.org on April 19, 2015. © 2014 American Association for Cancer Research.

Published OnlineFirst April 10, 2014; DOI: 10.1158/2326-6066.CIR-13-0143

syngeneic mice, concomitant with an early appearance of mature DCs in TDLNs. We used SeV/dF vectors for the gene transduction of vaccine cells because they have relatively higher capacities in terms of gene transduction, induction of antitumor immunity, and safety (6, 15). Expression microarray analyses of the GM-CSF–sensitized CD86$^+$ DCs revealed increased expression of the TLR7–IRF7 pathway components, which induce type I IFN production in pDCs (5). Furthermore, the addition of imiquimod was found to be an effective potential approach to improve the antitumor effects of GVAX therapy (Fig. 4).

As LLC cells have been considered as poorly immunogenic in lung cancer (16), it was surprising that tumor challenge with LLC/SeV/GM cells markedly impaired its tumorigenicity with complete tumor disappearance in half of the mice tested (Fig. 1). In addition, prophylactic vaccination with irLLC/SeV/GM cells also significantly inhibited subsequent tumor challenge with LLC cells (Supplementary Fig. S6). However, therapeutic vaccination using irLLC/SeV/GM cells alone failed to exert significant antitumor immunity (Fig. 4C). We, therefore, attempted to potentiate the therapeutic antitumor effects of irLLC/SeV/GM cells through scrutinizing the gene expression signature of GM-CSF–sensitized DCs in TDLNs from mice that strongly rejected the tumor challenge with LLC/SeV/GM cells. We confirmed that GM-CSF facilitated the maturation of DCs into antigen-presenting cells with enhanced ability to prime naïve T cells to proliferate, and to increase expression of CD80, CD86, MHC class I, MHC class II, and CD40 (Fig. 2B and Supplementary Fig. S7), consistent with the previous finding that GM-CSF promotes DCs maturation and differentiation (17). Herein, transcriptome analyses revealed that GM-CSF also modulated signal transduction in pDCs by upregulation of the TLR7–IRF7 pathway related to type I IFN production (Fig. 3), consistent with a previous report that GM-CSF stimulation upregulated TLR7 expression in mouse immune cells (18). Our observation that the pDC subset was markedly increased in GM-DCs from TDLNs was unexpected, as the GM-CSF receptor is mainly expressed on CD34$^+$ progenitor cells and myeloid cells (19, 20), and GM-CSF administration preferentially expands CD11b$^+$ cDC (21, 22) and inhibits pDC differentiation (23). However, recent studies showing that pDC precursors differentiated to CD11b$^+$MHC II^{high} cDCs by GM-CSF stimulation (24), and the identification of GM-CSF as a novel activator of pDCs revealed by systematic analysis of cytokine receptors (25), may explain the increase of GM-CSF–sensitized pDC subsets in TDLNs (Fig. 3D). In the development of active immunotherapeutic strategies, much attention has been focused on CD11b$^+$ cDC-based vaccines that have failed to induce sufficient clinical efficacy (26), as pDCs are considered to be involved in the maintenance of antitumor tolerance (27) and to be inversely correlated with prognosis in patients with cancer (28, 29). However, pDC subsets can be pivotal players in TAA-specific antitumor immune responses by functioning as antigen-presenting cells (30) that use distinct MHC class II antigen-presentation molecules (31), leading to the effective priming of naïve CD4$^+$ T cells (32), and cross-present antigens with an efficiency comparable with CD11b$^+$ cDCs (33), implicating their potential as promising antigen-presenting cells for cancer immunotherapy. Indeed, imiquimod or CpG, a TLR9 agonist, reverted immunotolerant pDCs to antitumor pDCs (34), resulting in clinical antitumor effects (35, 36). Importantly, results of our *in vivo* experiments using pDC depletion and/or IFNAR$^{-/-}$ mice demonstrated the positive impact of the pDC subset and/or type I IFN signaling on the effective generation of GM-CSF–induced antitumor immunity (Fig. 3E and F). Thus, there may be a functional dichotomy in pDC biology between immune tolerance and antitumor phenotype, where their redirection is dependent on the tumor microenvironment.

Imiquimod, a TLR7 ligand, could be regarded as the most effective adjuvant among all approved immunomodulators based on the following: (i) topical imiquimod is currently FDA approved with a good safety profile; (ii) it potently activates antigen-presenting cells to release type I IFNs and Th1-skewing cytokines; and (iii) imiquimod treatment leads to CCL2-dependent recruitment of pDCs and their transformation into killer DCs (37). The underlying mechanism of substantial antitumor efficacy by the combined vaccination may be due to generation of functionally mature pDCs in TVSs and TDLNs (Fig. 5A and Supplementary Fig. S4). IFNα, mainly produced from pDCs upon exposure to viruses via TLR7 or TLR9 (38), acts directly on memory T cells, which potentiate the antigen presentation and cross-priming capacities of CD11b$^+$ cDCs (39, 40). We detected CD9$^+$ pDCs, which produce abundant IFNα (14), in TDLNs from mice injected with ir.LLC/SeV/GM cells (Fig. 5C and D). Furthermore, GM-CSF–sensitized pDCs expressed higher CD86 and Siglec-H (Fig. 5B), a regulator of pDC differentiation and CD8$^+$ T-cell responses (13, 41). Moreover, pDCs activated with GM-CSF plus imiquimod further enhanced the proliferation of CD8$^+$ T cells (Fig. 5F), indicating that GM-CSF–activated pDCs with or without imiquimod could serve as functional antigen-presenting cells to prime the potent generation of TAA-specific adaptive immunity. ELISPOT assay demonstrated that the number of IFNγ-producing splenocytes from mice treated with irLLC/SeV/GM cells plus imiquimod was increased compared with control mice (data not shown). Indeed, depletion assays revealed that CD4$^+$ and CD8$^+$ T cells significantly contributed to the augmentation of the antitumor efficacy by combination GVAX therapy (Fig. 5G), thus reflecting the imiquimod-driven accelerated TAA-specific Th1 responses.

Although other researchers showed that the addition of imiquimod negates the antitumor efficacy of a GM-CSF–based vaccine (42), these conflicting results may stem from the difference in doses and administration schedule. It is noteworthy that the ability of imiquimod to potentiate the antitumor effect of GVAX therapy in two different types of cancers and in two different host strains might confirm the generality of our findings (Fig. 4C and D).

In conclusion, we, for the first time, elucidated that the beneficial roles of the pDCs and relevant type I IFN pathway

Downloaded from cancerimmunolres.aacrjournals.org on April 19, 2015. © 2014 American Association for Cancer Research.

Published OnlineFirst April 10, 2014; DOI: 10.1158/2326-6066.CIR-13-0143

in GM-CSF–induced antitumor immunity and that the combinational use of imiquimod with GVAX therapy produced synergistic antitumor effects, underscoring its potential as a promising approach for the treatment of cancer.

Disclosure of Potential Conflicts of Interest

No potential conflicts of interest were disclosed.

Authors' Contributions

Conception and design: M. Narusawa, H. Inoue, Y. Matsumura, K. Tani
Development of methodology: M. Narusawa, H. Inoue, Y. Matsumura, M. Inoue, M. Hasegawa
Acquisition of data (provided animals, acquired and managed patients, provided facilities, etc.): M. Narusawa, H. Inoue, C. Sakamoto, Y. Matsumura, A. Watanabe, K. Tani
Analysis and interpretation of data (e.g., statistical analysis, biostatistics, computational analysis): M. Narusawa, H. Inoue, Y. Matsumura, T. Inoue, S. Miyamoto
Writing, review, and/or revision of the manuscript: M. Narusawa, H. Inoue, A. Takahashi, Y. Tanaka, K. Takayama, T. Okazaki, Y. Nakanishi
Administrative, technical, or material support (i.e., reporting or organizing data, constructing databases): Y. Matsumura, T. Inoue, Y. Miura, M. Hasegawa, K. Tani
Study supervision: H. Inoue, Y. Matsumura, A. Takahashi, Y. Hijikata, T. Okazaki, K. Tani

Acknowledgments

The authors thank Michiyo Okada, Michiko Ushijima, Yosuke Yokota, and Haruka Nabeta for excellent technical assistance, and Kaori Yasuda and Atsushi Doi for performing the cDNA microarray analysis. The authors also thank Katsuaki Sato for valuable discussion.

Grant Support

This work was supported by JSPS KAKENHI grant number 21790773 and a grant for students through the Kyushu University Foundation research grant program.

The costs of publication of this article were defrayed in part by the payment of page charges. This article must therefore be hereby marked *advertisement* in accordance with 18 U.S.C. Section 1734 solely to indicate this fact.

Received September 5, 2013; revised February 5, 2014; accepted March 3, 2014; published OnlineFirst April 10, 2014.

References

1. Dranoff G, Jaffee E, Lazenby A, Golumbek P, Levitsky H, Brose K, et al. Vaccination with irradiated tumor cells engineered to secrete murine granulocyte-macrophage colony-stimulating factor stimulates potent, specific, and long-lasting anti-tumor immunity. Proc Natl Acad Sci U S A 1993;90:3539–43.
2. Tani K, Azuma M, Nakazaki Y, Oyaizu N, Hase H, Ohata J, et al. Phase I study of autologous tumor vaccines transduced with the GM-CSF gene in four patients with stage IV renal cell cancer in Japan: clinical and immunological findings. Mol Ther 2004;10:799–816.
3. Longo DL. New therapies for castration-resistant prostate cancer. N Engl J Med 2010;363:479–81.
4. Li HO, Zhu YF, Asakawa M, Kuma H, Hirata T, Ueda Y, et al. A cytoplasmic RNA vector derived from nontransmissible Sendai virus with efficient gene transfer and expression. J Virol 2000;74:6564–9.
5. Honda K, Yanai H, Negishi H, Asagiri M, Sato M, Mizutani T, et al. IRF-7 is the master regulator of type-I interferon-dependent immune responses. Nature 2005;434:772–7.
6. Inoue H, Iga M, Nabeta H, Yokoo T, Suehiro Y, Okano S, et al. Non-transmissible Sendai virus encoding granulocyte macrophage colony-stimulating factor is a novel and potent vector system for producing autologous tumor vaccines. Cancer Sci 2008;99:2315–26.
7. Yoneyama H, Matsuno K, Toda E, Nishiwaki T, Matsuo N, Nakano A, et al. Plasmacytoid DCs help lymph node DCs to induce anti-HSV CTLs. J Exp Med 2005;202:425–35.
8. Yokota Y, Inoue H, Matsumura Y, Nabeta H, Narusawa M, Watanabe A, et al. Absence of LTB4/BLT1 axis facilitates generation of mouse GM-CSF–induced long-lasting antitumor immunologic memory by enhancing innate and adaptive immune systems. Blood 2012;120:3444–54.
9. Sadler AJ, Williams BR. Interferon-inducible antiviral effectors. Nat Rev Immunol 2008;8:559–68.
10. Gilliet M, Cao W, Liu YJ. Plasmacytoid dendritic cells: sensing nucleic acids in viral infection and autoimmune diseases. Nat Rev Immunol 2008;8:594–606.
11. Colonna M, Trinchieri G, Liu YJ. Plasmacytoid dendritic cells in immunity. Nat Immunol 2004;5:1219–26.
12. Akira S, Hemmi H. Recognition of pathogen-associated molecular patterns by TLR family. Immunol Lett 2003;85:85–95.
13. Takagi H, Fukaya T, Eizumi K, Sato Y, Sato K, Shibazaki A, et al. Plasmacytoid dendritic cells are crucial for the initiation of inflammation and T cell immunity *in vivo*. Immunity 2011;35:958–71.
14. Bjorck P, Leong HX, Engleman EG. Plasmacytoid dendritic cell dichotomy: identification of IFN-alpha producing cells as a phenotypically and functionally distinct subset. J Immunol 2011;186:1477–85.
15. Shi L, Chen J, Zhong Q, Li M, Geng P, He J, et al. Inactivated Sendai virus strain Tianjin, a novel genotype of Sendai virus, inhibits growth of murine colon carcinoma through inducing immune responses and apoptosis. J Transl Med 2013;11:205.
16. Sumimoto H, Tani K, Nakazaki Y, Tanabe T, Hibino H, Hamada H, et al. GM-CSF and B7-1 (CD80) co-stimulatory signals co-operate in the induction of effective anti-tumor immunity in syngeneic mice. Int J Cancer 1997;73:556–61.
17. Wada H, Noguchi Y, Marino MW, Dunn AR, Old LJ. T cell functions in granulocyte/macrophage colony-stimulating factor deficient mice. Proc Natl Acad Sci U S A 1997;94:12557–61.
18. Yang H, Wei J, Zhang H, Lin L, Zhang W, He S. Upregulation of Toll-like receptor (TLR) expression and release of cytokines from P815 mast cells by GM-CSF. BMC Cell Biol 2009;10:37.
19. Barreda DR, Hanington PC, Belosevic M. Regulation of myeloid development and function by colony stimulating factors. Dev Comp Immunol 2004;28:509–54.
20. Kingston D, Schmid MA, Onai N, Obata-Onai A, Baumjohann D, Manz MG. The concerted action of GM-CSF and Flt3-ligand on *in vivo* dendritic cell homeostasis. Blood 2009;114:835–43.
21. Mausberg AK, Jander S, Reichmann G. Intracerebral granulocyte-macrophage colony-stimulating factor induces functionally competent dendritic cells in the mouse brain. Glia 2009;57:1341–50.
22. Daro E, Pulendran B, Brasel K, Teepe M, Pettit D, Lynch DH, et al. Polyethylene glycol-modified GM-CSF expands CD11b(high)CD11c(high) but notCD11b(low)CD11c(high) murine dendritic cells *in vivo*: a comparative analysis with Flt3 ligand. J Immunol 2000;165:49–58.
23. Esashi E, Wang YH, Perng O, Qin XF, Liu YJ, Watowich SS. The signal transducer STAT5 inhibits plasmacytoid dendritic cell development by suppressing transcription factor IRF8. Immunity 2008;28:509–20.
24. Schlitzer A, Loschko J, Mair K, Vogelmann R, Henkel L, Einwachter H, et al. Identification of CCR9$^-$ murine plasmacytoid DC precursors with plasticity to differentiate into conventional DCs. Blood 2011;117:6562–70.
25. Ghirelli C, Zollinger R, Soumelis V. Systematic cytokine receptor profiling reveals GM-CSF as a novel TLR-independent activator of human plasmacytoid predendritic cells. Blood 2010;115:5037–40.
26. Banchereau J, Palucka AK. Dendritic cells as therapeutic vaccines against cancer. Nat Rev Immunol 2005;5:296–306.
27. Munn DH, Sharma MD, Hou D, Baban B, Lee JR, Antonia SJ, et al. Expression of indoleamine 2,3-dioxygenase by plasmacytoid dendritic cells in tumor-draining lymph nodes. J Clin Invest 2004;114:280–90.
28. Labidi-Galy SI, Sisirak V, Meeus P, Gobert M, Treilleux I, Bajard A, et al. Quantitative and functional alterations of plasmacytoid dendritic cells

Downloaded from cancerimmunolres.aacrjournals.org on April 19, 2015. © 2014 American Association for Cancer Research.